

A broken solar type II radio burst induced by a coronal shock propagating across the streamer boundary

X. L. Kong^{1,2}, Y. Chen¹, G. Li^{3,1}, S. W. Feng¹, H. Q. Song¹, F. Guo⁴, and F. R. Jiao¹

ABSTRACT

We discuss an intriguing type II radio burst that occurred on 2011 March 27. The dynamic spectrum was featured by a sudden break at about 43 MHz on the well-observed harmonic branch. Before the break, the spectrum drifted gradually with a mean rate of about -0.05 MHz s^{-1} . Following the break, the spectrum jumped to lower frequencies. The post-break emission lasted for about three minutes. It consisted of an overall slow drift which appeared to have a few fast drift sub-bands. Simultaneous observations from the Solar TERrestrial RELations Observatory (STEREO) and the Solar Dynamics Observatory (SDO) were also available and are examined for this event. We suggest that the slow-drift period before the break was generated inside a streamer by a coronal eruption driven shock, and the spectral break as well as the relatively wide spectrum after the break is a consequence of the shock crossing the streamer boundary where density drops abruptly. It is suggested that this type of radio bursts can be taken as a unique diagnostic tool for inferring the coronal density structure, as well as the radio emitting source region.

Subject headings: shock waves — Sun: activity — Sun: corona — Sun: radio radiation

1. Introduction

It is generally believed that type II radio bursts are caused by electrons accelerated at magnetohydrodynamic shocks driven by solar eruptions. In the dynamic spectra recorded

¹Shandong Provincial Key Laboratory of Optical Astronomy and Solar-Terrestrial Environment, School of Space Science and Physics, Shandong University at Weihai, Weihai, China 264209; yaochen@sdu.edu.cn

²State Key laboratory for Space Weather, Center for Space Science and Applied Research, Chinese Academy of Sciences, Beijing 100190, China

³Department of Physics and CSPAR, University of Alabama in Huntsville, Huntsville, AL 35899, USA

⁴Department of Planetary Sciences and Lunar and Planetary laboratory, University of Arizona, Tucson, AZ 85721, USA

by ground-based or space-borne radio spectrographs, type II bursts are often identified as narrow stripes in the metric to kilometric wavelength range which drift gradually from high frequency to low frequency due to an outward propagation of the electron source along with the shock (Wild 1950; Nelson & Melrose 1985). Sometimes two stripes with a frequency ratio about two are observed, being interpreted as the fundamental (F) and the second harmonic (H) emissions generated via plasma radiation mechanism at frequencies determined by the local plasma density (Ginzburg & Zhelezniakov 1958). The frequency drift rate of type II radio bursts can be used to obtain the shock propagation speed by converting the emission frequencies into coronal heights assuming a coronal density model (e.g., Reiner et al. 2003; Vršnak et al. 2001, 2002, 2004; Cho et al. 2007, 2011).

Complex and sometime elusive morphological features are frequently present in type II dynamic spectra. For instance, the aforementioned F and H branches may further split into two bands causing the well-known band-splitting phenomena (Smerd et al. 1974, 1975; Vršnak et al. 2001). There may exist two or more type II bursts that occur closely in time, referred to as multi-band events. These can be due to different shocks of different solar drivers (i.e., flares or CMEs) or different locations along a single shock front (Robinson & Sheridan 1982; Nelson & Melrose 1985; Mancuso & Raymond 2004; Shanmugaraju et al. 2005; Cho et al. 2011). It has also been known that many type II bursts exhibit intermittent emissions rather than a continuous band. Indeed, according to Cane & Erickson (2005), the most common type II bursts observed by Wind/WAVES (Bougeret et al. 1995) belongs to the group of “blobs and bands”. In addition, there are type II bursts that have “herringbones”, which are short-lasting and rapid-drifting emissions that extend to both higher and lower frequencies from an overall slow-drifting backbone structure (Roberts 1959; Cairns & Robinson 1987; Zlobec et al. 1993; Mann & Klassen 2005). Apparently, these complex spectral features are the consequences of the underlying physical processes involved in shock formation and propagation, electron acceleration, and the radio emitting processes. Understanding these features can be challenging, but nevertheless are very helpful to better decipher the underlying physical processes. We note that simultaneous high-resolution and high-cadence solar imaging observations such as those from the Solar TERrestrial RELations Observatory (STEREO; Kaiser et al. 2008) and the Solar Dynamics Observatory (SDO; Pesnell et al. 2011) can provide valuable information on the eruption driver which can be crucial in interpreting the observed radio bursts.

In a recent study, Feng et al. (2012) explored the possibility of using type II spectral shape to infer the location of the shock-radio emission source. They reported the presence of spectral bumps in two solar eruption events and proposed that the spectral bumps were caused by the shock-radio emitting region (presumably a portion of the CME-driven shock) entering the dense streamer structure from a less dense coronal material outside of the

streamer. In this study, we examine another metric type II event that occurred on 2011 March 27 which showed different morphological features as those studied in Feng et al. (2012). The paper is organized as follows. In section 2 we describe the major features of the type II spectrum, including a sudden drop of the frequency and the following intermittent fast drifting. Details of the associated solar eruption are also presented. In section 3 we analyze the radio dynamic spectrum and the coronal imaging data to propose a scenario for the origin of the observed radio burst. The last section provides our conclusions and discussion.

2. Observations

Between 00:00-01:00 UT on 2011 March 27, several ground-based stations, including Culgoora (Prestage et al. 1994), Learmonth, and BIRS (Bruny Island Radio Spectrometer; Erickson 1997), recorded the type II event. In this paper, we mainly use the data of BIRS which has a frequency range of 6-62 MHz and a time cadence of 3 seconds. We also make use of full-disk imaging and coronagraph observations from the STEREO and the SDO satellite. These instruments have unprecedented high cadences and sensitivities: the Extreme-Ultraviolet Imagers (EUVI) on the Sun Earth Connection Coronal and Heliospheric Investigation (SECCHI/STEREO; Howard et al. 2008) has a field of view (FOV) extending to $1.7 R_{\odot}$ and a time cadence of 2.5 minutes in 195 \AA ; the FOV and time cadence of the inner coronagraph (COR1) of SECCHI are $1.4-4 R_{\odot}$ and 5 minutes; the FOV and time cadence of the Atmospheric Imaging Assembly (AIA; Lemen et al. 2011) onboard SDO (we use the 304 \AA and the 171 \AA channels) are $0-1.5 R_{\odot}$ and 12 seconds.

2.1. A broken type II dynamic spectrum

Figure 1 displays the GOES soft X-ray flux and the associated radio dynamic spectrum recorded by BIRS in the range 10-62 MHz and Learmonth in the range of 62-75 MHz. Type III bursts occurred between 00:13:30 UT and 00:16:30 UT, that were temporally coincident with the X-ray flux due to the C3.2 flare are clearly seen. The type II burst started about 10 minutes later when the X-ray flux already declined to the background level. Before 00:30 UT, both the F and H branches can be identified. After this time, the radio signals below 25 MHz became intermittent as a consequence of ionospheric absorption and radio noises. Nevertheless, we can still discern a few patches of emissions in the fundamental branch. Two such patches are indicated by the white arrows in the figure, one at 00:34 UT ($\sim 19 \text{ MHz}$) and the other at 00:35:30 UT ($\sim 14 \text{ MHz}$). Comparing to the fundamental branch, the

harmonic branch (40-25 MHz) is more pronounced and clear and contains more recognizable details. Therefore we will consider only the Harmonic component of the emission in this study.

The center of the H branch started around 60 MHz. The most prominent feature of the H branch is the change of the spectral slope and the presence of a breaking point separating the whole spectrum into two parts. The break occurred at 00:33 UT and ~ 43 MHz. Before the break, the spectrum drifted gradually in six minutes from 60 to 43 MHz with a mean drift rate of about -0.05 MHz s^{-1} . After the break, the spectrum continues as a type II burst at lower frequencies. There was no gap in time and frequency between the emission before the break and that after the break, and the overall emission profiles before and after the break are very similar although there are differences in details. Because of these, we suggest that the whole radio spectrum corresponds to one single underlying physical process and the sudden drop in frequency is due to a sudden change of the background environment (e.g. the density). However, other possibilities of interpretation such as multiple type II bursts (e.g. Nelson & Melrose 1985) and two distinct type II sources by a single CME-driven shock (e.g. Mancuso & Raymond 2004) cannot be ruled out. The after-break spectrum lasted for about three minutes. The bandwidth after the break was somewhat wider than that before the break (> 10 MHz). The overall drift after the break seemed to be slower than that before the break, but a careful examination suggests that it was composed of a few fast-drifting bands. The first such band drifted rapidly at the spectral break from 43 MHz to nearly 27 MHz in about one minute with an average drift of -0.27 MHz s^{-1} . An adjacent fast-drift band can be also identified from Figure 1 which has a similar frequency range and drift rate.

It should be pointed out that these fast-drifting bands are different from the usual herringbone structures that are commonly seen in type II radio bursts. Indeed, in this event, herringbone structures can be identified between 00:27 UT - 00:33 UT before the spectral break. These structures are caused by fast electrons moving along field lines and therefore are practically “vertical” structures (i.e. with a very fast frequency drift). We are not concerned with these structures in this study.

The solid lines in Figure 1 are given by fitting the pre-break spectrum with a two-fold Newkirk density model of the ambient corona (Newkirk 1961). The shock speed is taken to be 600 km s^{-1} . The dashed line is an extension of the fitting to the harmonic branch. From the fitting, we can deduce that the type II started at $\sim 2.0 R_{\odot}$ and the spectral break was located at $\sim 2.3 R_{\odot}$ (using the two-fold Newkirk density model). In the following, we will compare the inferred radio emitting heights from the fitting of the radio spectrum to those from direct imaging observation.

2.2. STEREO and SDO observations of the eruption

In this subsection, we discuss relevant imaging observations of the 2011 March 27 event.

On 2011 March 27, STEREO A and B were separated by about 176° , with STEREO A $\sim 89^\circ$ ahead the SDO satellite and STEREO B $\sim 95^\circ$ behind. As such, these three spacecraft formed a nearly-perfect “T” configuration, allowing us to observe the eruption from both head-on and side-ways. Before presenting the details of the eruptive processes, we first describe the overall magnetic and morphological features relevant to our study.

In Figure 2, we show the magnetic field configurations as obtained from the potential-field source-surface (PFSS; Schatten et al. 1969; Schrijver & DeRosa 2003) model based on the measurements with SDO/Helioseismic and Magnetic Imager (HMI; Schou et al. 2011) for the Carrington Rotation (CR) 2108. The field lines are adjusted to the three viewing angles of the spacecraft, respectively. Coronal images from the COR1 and the EUVI instruments onboard STEREO B and A at about 00:10 UT are also shown in Figures 2(a) and 2(c).

According to Figure 2(b), there existed several active regions on the solar disk. The source of our event was NOAA active region (AR) 11176 at S16E04 (from solarmonitor.org) as viewed from the earth (SDO) and denoted by the yellow arrows on the EUVI data. Clearly, the event was observed by SDO from the front as a solar disk event and by STEREO A/B from two sides as a limb event. This allows us to obtain simultaneously the evolutionary details of the AR at the early stage of the eruption and its coronal responses, which are free of projection effects that are often encountered from observations at a later stage.

The equatorial streamer corresponds to the large-scale closed field lines striding over ARs 11176 and 11177. The vertical black lines atop the streamer at $2.3 R_\odot$ in Figure 2(a) and (c) indicate the estimated location of the streamer cusp. The dashed lines, which lie about 4 degrees above the equator, represent the center of the streamer. The vertical black arrows on the COR1 data point to a coronal cavity structure. The cavity reached a height of $\sim 1.8 R_\odot$ with a width estimated to be about $0.05 R_\odot$. Coronal cavities are usually regarded as prominence supporting structures with relatively low density and strong magnetic field (see Tandberg-Hanssen 1974, 1995; Engvold 1989; Gibson et al. 2006). This is consistent with the SDO and STEREO observations of this event.

We now examine the pre-eruption source properties and how the eruption disturbed the surrounding plasma environment. The upper panels of Figure 3 show the SDO data for the source region. The HMI field measurements at 00:00:32 UT are shown in Figure 3(a), and the AIA 304 Å image at 00:00:08 UT in Figure 3(b), both with an FOV of $0.3 \times 0.3 R_\odot$. We can see that the source region was featured by a S-shape bright structure as viewed in 304 Å, which is above the bipolar magnetic field region separated by a neutral line with similar

shape. There were many dark filament structures near the S-shape structure, possibly related to the cavity discussed above. Two minutes after the first observation of the eruption by AIA at 00:08:07 UT, many overlying large-scale loop structures were observed in the 171 Å wavelength as shown in Figure 3(c) at 00:10:00 UT. At this time, the large-scale loop structures have not been affected by the eruption.

The eruption started with a sudden brightening of the S structure which led to the outward ejection of some bright materials, as seen in Figure 3(c). The whole process can be viewed from the corresponding online animation. It can be seen that the ejection resulted in significant disturbances to both the underlying and overlying loop structures. A weak yet recognizable disturbance was observed to spread out to the surrounding corona. It seems that some overlying arcades were opened by the ejected materials as seen from Figure 3(d) at 00:16:00 UT. In the mean time, the eruption was well observed by the EUVI instruments as a limb event. The corresponding observations by STEREO B are shown in the lower panels of Figure 3. Figure 3(f) was taken when the eruption was first observed, and Figure 3(e) was taken 5 minutes earlier and Figure 3(g) 2.5 minutes later. We can see that the ejecta moved outwards along a highly-inclined direction with an angle of $\sim 60^\circ$ to the radial direction, as indicated by the white arrow in Figure 3(g). In other words, the ejecta basically propagated out along the direction of the confining field lines in the early stage. From the last panel and the corresponding online animation, the ejection opened the confining arcades, and escaped from the crossing tips of the EUV rays beneath the aforementioned equatorial streamer. The ray tips, as marked by the “+” symbol, was located at $\sim 0.25 R_\odot$ above the equator and $\sim 1.55 R_\odot$ from the solar center. These observations are consistent with those observed by AIA. It should be mentioned that considerable materials falling back towards the sun were observed after 00:30 UT as can be seen from the online AIA 304 Å animation. We will discuss this further in the following.

The impact of the ejecta to the outer corona was observed with the COR1 coronagraphs. The corresponding original image at 00:15 UT and the running difference images from 00:20 UT to 00:40 UT obtained by COR1B in an FOV of $2.0 \times 2.0 R_\odot$ are shown in the left side of Figure 4. The eruption was first observed at 00:20 UT as an outward propagating bright front sweeping through the streamer structure. The dashed and solid lines are the same as those plotted in Figure 2 representing the possible height of the streamer cusp and the pre-disturbed streamer axis. We can see that when first observed by COR1B the disturbance front was located at about $1.80 R_\odot$, and reached $2.02 R_\odot$ and $2.24 R_\odot$ at 00:25 UT and 00:30 UT. The front crossed the solid line, i.e., the estimated height of the streamer cusp, between 00:30 UT and 00:35 UT. It further propagated out and reached $2.7 R_\odot$ at 00:40 UT, and became diffusive and hardly recognizable after 00:55 UT.

As viewed from the online animation, the streamer cavity, indicated by the black arrows on the COR1 images in Figure 2, started to get slightly larger since 00:25 UT and moved upwards slowly. The mean speed was only about 80 km s^{-1} from 00:25 UT to 01:00 UT, much lower than that of the front. The cavity stopped to rise at about 01:30 UT and fell back to its pre-eruption height at about 02:30 UT. From the nearly identical locations of the cavity and the EUVI ray tips through which the materials escaped, we speculate that the erupted materials run into the cavity and/or surrounding arcades and were then confined there. The fact that the cavity did not further expand and eventually fell back suggests that the bright front observed by the STEREO coronagraphs represents an outward-propagating disturbance, rather than erupting coronal material. Careful Examination of both the COR1 and COR2 images revealed that the equatorial streamer later returned to its pre-eruption state without suffering any disruption. There was also no apparent signatures of mass ejection trailing the outward-propagating disturbance. This is also consistent with the rapid weakening of the disturbance front and the presence of considerable falling-back material as reported previously.

The sequence of this eruption can be summarized as the following: The initial eruption was triggered from an AR located at one foot of the streamer structure. The eruption followed along the highly-inclined pre-existing coronal arcades beneath the streamer and resulted in a bright outward-moving disturbance front (likely a shock) sweeping through the streamer structure. There was not enough material/energy contained in the eruption and the the ejected material were stuck within the streamer and eventually fell back to the sun.

3. Physical origins of the broken dynamic spectrum

We now examine the physical origins accounting for the broken feature of the type II radio burst observed in this event. To achieve this, we first compare the heights measured from the STEREO observations with that deduced from the dynamic spectrum using the two-fold Newkirk density model. The fitting to the radio data before the break was shown in Figure 1, yielding a shock speed of 600 km s^{-1} . The deduced radio-emitting shock heights have been shown in the right side of Figure 4 as open circles. The heights of the disturbance front measured from the STEREO observations are also plotted as squares for COR1 and triangles for EUVI in blue (red) for STEREO A (B). Since it is a limb event from both STEREO A and B, measurement uncertainties are small and estimated to be less than $0.05 R_{\odot}$ (about 10 pixels). We can see that the two sets of heights agree nicely with each other. The linearly-fitted propagation speeds of the front are 681 and 499 km s^{-1} for EUVI and COR1 of STEREO A; and 720 and 512 km s^{-1} for STEREO B. These speeds are consistent

with that obtained by the above radio fitting method. Based on these comparisons, we suggest that the type II burst was driven by the shock corresponding to the bright disturbance front observed by STEREO.

We now examine the cause for the spectral break. The break occurred at 00:33 UT between the images shown in Figure 4(d) (00:30 UT) and 4(e) (00:35 UT). During this period, the shock front crossed the black line located at $2.3 R_{\odot}$ atop the streamer. Using the two-fold Newkirk density model, a harmonic frequency of 43 MHz also corresponds to $2.3 R_{\odot}$. Therefore it is conceivable that the spectral break was caused by the shock crossing the streamer boundary, and the pre-break spectrum was emitted inside the streamer. This is consistent with the imaging observations that the event erupted at one foot of the streamer and propagated towards the center of the streamer.

Across the streamer boundary, the density drops faster than that described by, e.g. the Newkirk model (which has a radial dependence $\sim 10^{4.32/r}$). Such a larger density gradient will lead to a faster drift of the type II radio burst. Furthermore, since type II radio burst is expected to be sporadic and best described as “blobs and bands” (Cane & Erickson 2005), one expects to find several such fast drifting branches, each corresponding to a radio emission region, as the shock propagates through the streamer boundary. Indeed, this is what was observed in the radio spectrum after the break: there seems to be three sub-branches in the post-break radio spectrum, all with similar drift rates which are several-times faster than that inferred from a radial density drop with a radial shock speed of 600 km s^{-1} .

The process is further illustrated by the cartoons plotted in Figure 5. Figure 5(a) plots the magnetic field lines of the streamer and the locations of the shock fronts at various times. The transition layer from inside the dense streamer to the surrounding dilute solar wind is colored in yellow. The type II radio emission region is indicated by the red thick segment in Figure 5(a). To illustrate the intermittent feature of the type II radio burst, in Figure 5(b), we consider three points P, Q, R along the shock as the major radio emission sources. The shock front crossed the streamer cusp at a time between 00:30 UT and 00:35 UT. The spectral break was observed at 00:33 UT corresponding to the start of the transit of the radio source P across the streamer boundary. Before this time, all radio sources (P, Q and R) were inside the streamer. At 00:33 UT, Point P intersects with the transition layer at point A and later at A' (coming into the solar wind); Point Q intersects with the transition layer at points B and later at B'; and Point R intersects with the transition layer at points C and later at C'. The time sequence for these intersections, as drawn in Figure 5(b) and Figure 5(c), satisfies $t(A) < t(A') < t(B) < t(B') < t(C) < t(C')$, which is consistent with Figure 1. The radiation ended soon after the radio sources moved out of the transition layer, perhaps because the shock weakened in the faster solar wind. Indeed, since the solar wind is

less dense and the Alfvén speed is expected to be faster, the shock wave inside the streamer may “unshock” in the solar wind and fail to accelerate enough electrons to excite the type II bursts here. This is consistent with the short duration of the post-break emission. Also note the bandwidth before the break is governed by the density difference between P and R, which is considerably narrower than that after the break, since the post-break bandwidth involves a much faster density drop introduced by the streamer boundary.

Using the measurements of the shock speed, the radio frequency drift, and the temporal duration of the radio emission after the break, one can in principle deduce the thickness and drop rate of the electron density at the streamer boundary. In our event, we can see that the emission lasts for about 2 minutes after the spectral break, and the frequency of the H branch changes from about 40 to 25 MHz, corresponding to a density drop from about 5 to $2 \times 10^6 \text{ cm}^{-3}$. A shock with a speed of 600 km s^{-1} propagates a distance of about $0.1 R_{\odot}$ in 2 minutes. Considering the shock may not propagate perpendicularly across the streamer boundary, this distance should be considered as an upper limit of the radial distance of the above density drop. Also, it should be noted that the radio emission may stop before the shock fully cross the streamer boundary (see Figure 5). Therefore, the values estimated above may be smaller than the total density drop and the total thickness of the streamer boundary. In spite of these, these values are comparable to the electron density measurements across a coronal streamer at a similar height of $2.33 R_{\odot}$ in heliocentric distance by Strachan et al. (2002).

4. Discussion and Conclusions

In this paper we report an intriguing type II radio burst featured by a spectral break. The radio burst is likely caused by a coronal eruption driven shock sweeping through the streamer structure. The spectrum before the break looks like a typical type II radio burst with a gradually-drifting rate consistent with a shock speed of 600 km s^{-1} moving in a corona whose density profile can be well described by a two-fold Newkirk density model. The spectrum after the break is composed of several fast-drifting bands, which can be explained by shock moving across a transition layer that has a sharper density gradient. With this interpretation, the time of the spectral break indicates the time when the radio emission regions (along the shock) interact with the transition layer, therefore allowing us to use features in the type II radio bursts, which presumably has no spatial information on the underlying emission process, to deduce its location.

We also note that the event studied is featured by an outward-propagating shock front which was driven by the erupting coronal material during the early stage of the eruption.

The erupting material seemed to be confined within the overlying streamer arcades without escaping the corona. This is inferred from the following observations: first, the streamer, within which the eruption took place, showed no disruption as all; second, there were no observable signatures of mass ejection trailing the shock front from the coronagraph data; third, a streamer cavity, into which the ejected mass possibly ran, was disturbed yet did not erupt during the event; and fourth, there were considerable eruptive materials falling down towards the sun as observed in 304 Å by AIA.

This study suggests that the streamer structure can play a role in accelerating electrons and exciting type II radio bursts. The streamer is characterized by large-scale confining magnetic arcades in which the plasmas are basically quasi-static without measurable outflows (e.g., Strachan et al. 2002). Its density is also higher than the surrounding solar wind. Therefore, the Alfvén speed within the streamer is likely lower. These conditions favor the formation and strengthening of shocks driven by a coronal mass eruption. Furthermore, a collapsing geometry, presumably an efficient electron accelerator (e.g., Zlobec et al. 1993; Somov & Kosugi 1997; Magdalenic et al. 2002), can be formed when a shock sweeps through the closed magnetic arcades of a streamer. To our knowledge, similar events have not been reported before and our study is the first to examine spectral break of type II radial bursts and explain it as an eruption within a streamer. Further surveys to identify more events that exhibit similar spectral features involving a coronal streamer will be carried out in the future. Theoretical studies on the role of streamers in shock-induced electron acceleration and type II radio bursts will also be pursued.

We are grateful to STEREO/SECCHI, SDO/AIA, SDO/HMI and Learmonth teams for making their data available online. We thank Dr. Stephen White and Dr. Bill Erickson for providing the BIRS data. This work was supported by grants NSBRSF 2012CB825601, NNSFC 40825014, 40890162, 41028004, and the Specialized Research Fund for State Key Laboratory of Space Weather in China. H.Q. Song was also supported by NNSFC 41104113. Gang Li’s work at UAHuntsville was supported by NSF CAREER: ATM-0847719 and NSF SHINE: AGS-0962658.

REFERENCES

- Brueckner, G. E., Howard, R. A., Koomen, M. J., et al. 1995, *Sol. Phys.* 162, 357
- Bougeret, J. L., Kaiser, M. L., Kellogg, P. J., et al. 1995, *Space Sci. Rev.*, 71, 231
- Cairns, I. H. & Robinson, R. D. 1987, *Sol. Phys.*, 111, 365

- Cane, H. V. & Erickson, W. C. 2005, *ApJ*, 623, 1180
- Cho, K.-S., Lee, J., Gary, D. E., Moon, Y. J., & Park, Y. D., 2007, *ApJ*, 665, 799
- Cho, K.-S., Bong, S.-C., Moon, Y.-J., et al. 2011, *A&A*, 530, 16
- Engvold, O. 1989, in *Dynamics and Structures of Quiescent Prominences*, ed. E. R. Priest (Dordrecht: Reidel), 47
- Erickson, W. C. 1997, *Publication Astronomical Society of Australia*, 14, 3, 278-282
- Feng, S. W., Chen, Y., Kong, X. L., et al. 2012, submitted to *ApJ*
- Gibson, S. E., Foster, D., Burkepile, J., de Toma, G., & Stanger, A. 2006, *ApJ*, 641, 590
- Ginzburg, V. L., & Zhelezniakov, V. V. 1958, *SvA*, 2, 653
- Howard, R. A., Moses, J. D., Vourlidas, A., et al. 2008, *Space Sci. Rev.* 136, 67
- Kaiser, M. L., Kucera, T. A., Davila, J. M., et al. 2008, *Space Sci. Rev.* 136, 5
- Lemen, J. R., Title, A. M., Akin, D. J., et al. 2011, *Sol. Phys.*, in press
- Magdalenić, J., Vršnak, B., & Aurass, H. 2002, *Proc. 10th European Solar Physics Meeting, Solar Variability: From Core to Outer Frontiers*, ESA SP-506, 335
- Mancuso, S., & Raymond, J. C. 2004, *A&A*, 413, 363
- Mann, G., & Klassen, H. Y. 2005, *A&A*, 441, 319
- Nelson, G. J., & Melrose, D. B. 1985, in *Solar Radiophysics*, ed. D. J. McLean & N. R. Labrum (Cambridge: Cambridge Univ. Press), 333
- Newkirk, G. Jr. 1961, *ApJ*, 133, 983
- Pesnell, W. D., Thompson, B. J., Chamberlin, P. C. 2011, *Sol. Phys.*, in press
- Prestage, N. P., Luckhurst, R. G., Paterson, B. R., Bevins, C. S., & Yuile, C. G. 1994, *Sol. Phys.*, 150, 393
- Reiner, M. J., Vourlidas, A., Cyr, O. C. St., et al. 2003, *ApJ*, 590, 533
- Roberts, J. A. 1959, *Australien J. Phys.*, 12, 322
- Robinson, R. D., & Sheridan, K. V. 1982, *Proc. Astron. Soc. Aust.* 4, 392

- Schatten, K. H., Wilcox, J. M., & Ness, N. F. 1969, *Sol. Phys.*, 6, 442
- Schou, J., Scherrer, P. H., Bush, R. I., et al. 2011, *Sol. Phys.*, in press
- Schrijver, C. J., & Derosa, M. L., 2003, *Sol. Phys.*, 212, 165
- Shanmugaraju, A., Moon, Y.-J., Cho, K.-S., et al. 2005, *Sol. Phys.*, 232, 87
- Smerd, S. F., Sheridan, K. V., & Stewart, R. T., 1974, in *IAU Symp. 57*, ed. G. A. Newkirk, 389
- Smerd, S. F., Sheridan, K. V., & Stewart, R. T., 1975, *ApL*, 16, 23
- Somov, B. V., & Kosugi, T. 1997, *ApJ*, 485, 859
- Strachan, L., Suleiman, R., Panasyuk, A. V., Biesecker, D. A., & Kohl, J. L., 2002, *ApJ*, 571, 1008
- Tandberg-Hanssen, E. 1974, *Solar Prominences* (Dordrecht: Reidel)
- Tandberg-Hanssen, E. 1995, *The Nature of Solar Prominences* (Dordrecht: Kluwer)
- Vršnak, B., Aurass, H., Magdalenic, J., & Gopalswamy, N. 2001, *A&A*, 377, 321
- Vršnak, B., Aurass, H., Magdalenic, J., & Mann, G. 2002, *A&A*, 396, 673
- Vršnak, B., Magdalenic, J., & Zlobec, P. 2004, *A&A*, 413, 753
- Wild, J. P. 1950, *Aust. J. Sci. Res.*, A3, 541
- Zlobec, P., Messerotti, M., Karlicky, M., & Urbarz, H. 1993, *Sol. Phys.*, 144, 373

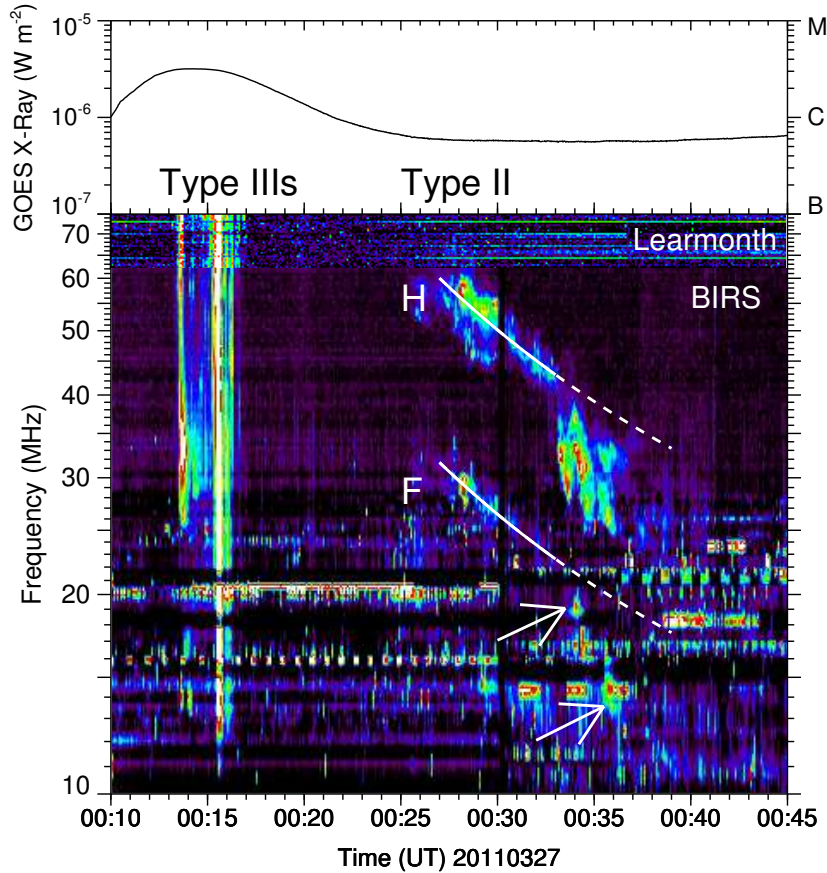


Fig. 1.— The upper panel plots the GOES soft X-ray flux, showing a C3.2 flare at the time of type IIIs onset. The lower panel is the radio dynamic spectrum from BIRS (10-62 MHz) and Learmonth (62-75 MHz). “F” and “H” stand for the fundamental and harmonic bands of type II burst, respectively. Solid lines are spectral fittings using the two-fold Newkirk density model and a shock of 600 km s^{-1} , the dashed line is the extension to the harmonic fitting. The two white arrows indicate the fundamental counterparts of the upper post-break emission.

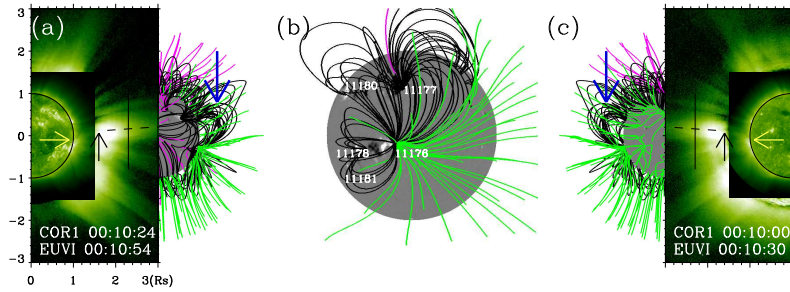


Fig. 2.— Magnetic field configurations as obtained from the PFSS model based on the measurements with SDO/HMI for the Carrington Rotation (CR) 2108. The field lines are already adjusted to the individual views of the three spacecraft. The closed lines are colored in black, and the open inward (outward) field lines in purple (green). Panels (a) and (c) also show coronal images from COR1 B/A and EUVI B/A 195 Å at about 00:10 UT with FOVs of $1.5 \times 3.0 R_{\odot}$ and $3.0 \times 6.0 R_{\odot}$. See text for more details.

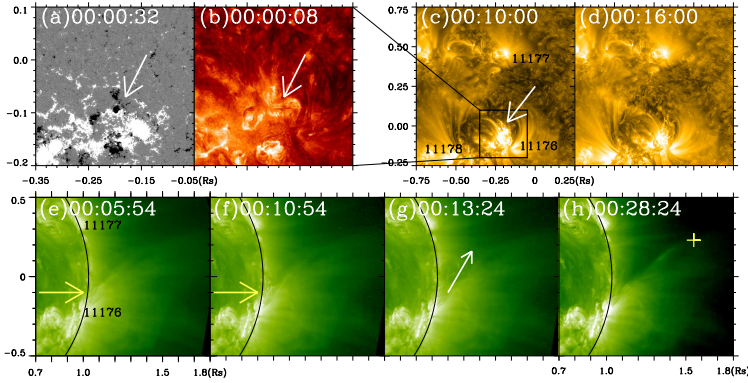


Fig. 3.— The upper panels show the SDO data observed from the front as a disk event. The HMI field measurements of the source region at 00:00:32 UT are shown in panel (a), and the AIA 304 Å image at 00:00:08 UT in panel (b). The location of the S-shape bright structure are indicated by the white arrows. Panels (c) and (d) are observed in 171 Å, showing many overlying large scale loop structures. The FOV for panels (c) and (d) is $1.0 \times 1.0 R_{\odot}$, and $0.3 \times 0.3 R_{\odot}$ for panels (a) and (b), indicated by the black box in panel (c). The lower panels show the EUVI B observation in 195 Å. The yellow arrows point to the eruption source region, i.e. AR11176, the same as in Figure 2. The white arrow in panel (g) indicates the direction the ejecta moving outwards in the early stage of eruption. The crossing tips of EUV rays is marked by the plus symbol in panel (h).

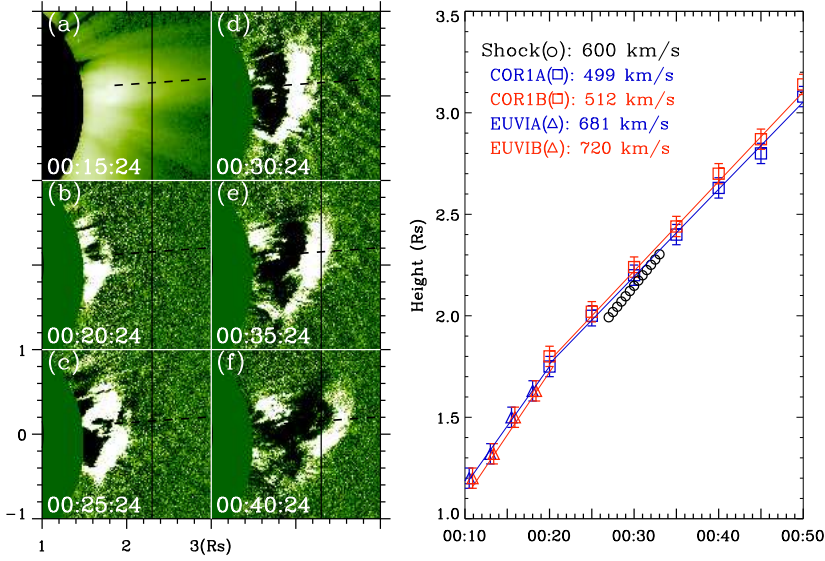


Fig. 4.— The left side are COR1B data between 00:15-00:40UT, with FOVs of $2.0 \times 2.0 R_{\odot}$. Panel (a) is the original image at 00:15 UT and the following are running difference images. The black dashed lines represent the center of the streamer, and the vertical black lines the estimated height of steamer cusp region, the same as in Figure 2. The right side plots the heights of the disturbance front measured from STEREO, with triangles for EUVI and squares for COR1 and in blue/red for STEREO A/B. The error bars indicate measurement uncertainties of the heights, estimated to be about $0.05 R_{\odot}$. The lines are obtained by linearly-fitting the EUVI and COR1 data points and the deduced propagation speeds are shown in the upper left corner. The deduced radio-emitting shock heights also are shown as open circles.

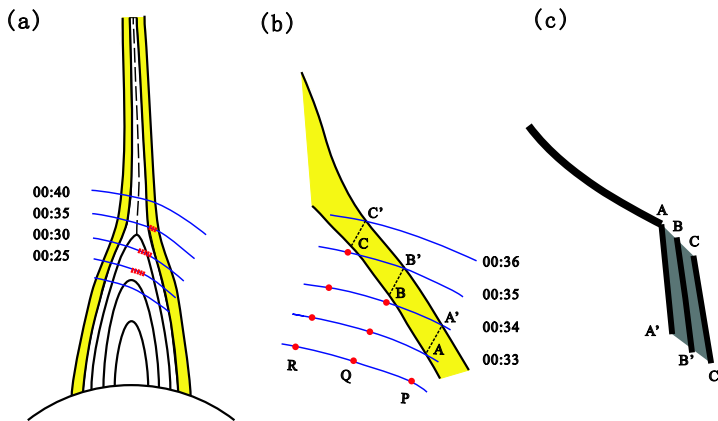


Fig. 5.— Cartoons illustrate the physical origin of the type II burst event. Panel (a) plots the magnetic field lines of the streamer and locations of the shock fronts, as black and blue curves, respectively. The streamer boundary is shaded in yellow. The radio emitting region is indicated by the red thick segment. Panel (b) illustrates the shock crossing the streamer boundary after 00:33 UT and panel (c) shows the corresponding spectral features.